Porous TiO2 layer for dye-sensitized solar cell formed with non-equilibrium 2D plasma induced by dielectric barrier discharge under atmospheric pressure

Porous TiO_2 layer for dye-sensitized solar cell formed with non-equilibrium 2D plasma induced by dielectric barrier discharge under atmospheric pressure

Masayuki Okuya*, Shinji Mayumi, Ryosuke Okumura, Yuki Masuda, and Isao Yagi

Electronics and Materials Science Course, Department of Engineering, Graduate School of Integrated Science and Technology, Shizuoka University, Hamamatsu 432-8561, Japan

E-mail: tcmokuy@shizuoka.ac.jp

A non-equilibrium 2D plasma was induced on the insulating plate by a dielectric barrier discharge under a flowing mixture of nitrogen and oxygen gases. A titanium-peroxo precursor to prepare an anatase TiO_2 film was irradiated with the plasma. The technique was applied to form a porous TiO_2 layer for a dye-sensitized solar cell (DSSC). We found the N−O metastable plasma induced under the higher nitrogen gas concentration played an important role in forming a porous TiO_2 layer, and promote a necking process between TiO_2 particles to reduce an internal resistance within the layer. The DSSC fabricated with the porous TiO_2 layer showed the maximum conversion efficiency of 3.7 %, which was lower than that of the general DSSC. However, with a non-equilibrium 2D plasma, the substrate temperature was kept below 80 ˚C during the plasma irradiation, which opens the way for subsequent progress in producing a DSSC for daily use.

1. Introduction

Plasma is one of the most attractive technologies developed for modern industry. Recently, plasma technology has made great progress, and it is used in the range of application from plasma display panels with several tens of meters wide to micro-machining techniques. Plasmas have many applications such as in surface modification [1, 2], sterilization in medical science [3-5], decomposition of nitrogen oxides in exhaust gases in environmental engineering [6-9], and plasma sintering. [10, 11] Plasmas induced under atmospheric pressure are roughly classified into two types: thermal equilibrium plasma represented by arc discharge, and non-equilibrium plasma represented by a glow discharge and a dielectric barrier discharge. Tens of thousands Kelvin electron temperature is a characteristic of non-equilibrium plasma, while the plasma decays rapidly in the system and the atmospheric gas close to the plasma is comparable to the room temperature. Non-equilibrium plasmas are induced in air [12, 13], micro-bubbles under the water [14-16], and the supercritical fluids [17-21] during the decades. Recently, a handy and compact device that induces micro-plasma is developing a new field in the industry. [22-26] Among the many plasma technologies, we focused on a dielectric barrier discharge in this study. A dielectric barrier discharge is easily created on the surface of an insulating plate by applying a high AC bias to both sides of the plate. The discharge spreads to the surface of the plate with high-energy electrons and induces a non-equilibrium 2D plasma on the electrode. We have succeeded in inducing a non-equilibrium 2D plasma by dielectric barrier discharge under atmospheric pressure and developed it into a film formation technique. [27, 28] In this technique, a planar plasma on the electrode is irradiated onto the surface of the precursor pre-coated on the substrate, and then the precursor is decomposed to form a ZnO film. Because the non-equilibrium plasma is confined within the area designed by the grid pattern on the electrode, and a high-energy plasma is irradiated on the selective exposed area on the substrate, the technique is convenient for direct patterning in film formation. [28] Additionally, with a non-equilibrium 2D plasma, the plasma treatment can be conducted only on the surface of the substrate without heating the entire volume. Therefore, a cheap and light plastic substrate with a low melting point can be used in this technique. We have already reported a coplanar-type electrode to induce a non-equilibrium 2D plasma. [28] In this electrode, as shown in Fig. 1(a), a high AC bias was applied along the surface of the insulating plate through metal grids on a commercial epoxy photoresist. Although the electrode can induce a fine planar plasma on several hundred nanometers of metal grid patterns, the energy of the plasma is relatively low. [28] This is because the epoxy plate for the photoresist cannot withstand the high AC bias. Additionally, the electrons in the discharge pass through the insulating plate twice to induce a surface discharge in this system, which severely reduces the output plasma energy. In contract, in this study, we employed a novel type of electrode, and the AC bias was applied vertically to the surface of the insulating plate as shown in Fig. 1(b). Compared with the conventional coplanar-type electrode, an AC bias is directly applied to the insulating plate, and a higher-energy plasma is induced on the novel electrode, which is

very useful in promoting chemical reactions of the precursor on the substrate during film formation.

For film preparation, we formed a porous TiO_2 layer on a fluorine-doped tin oxide (FTO) transparent conductive oxide (TCO) film by a spray pyrolysis deposition (SPD) technique, and applied the double-layer to dye-sensitized solar cells (DSSCs). [29-38] In forming a porous TiO_2 layer, an annealing process at 500 ˚C in air is required to produce a high-performance DSSC, which locks out a cheap plastic substrate and discourages our daily use of DSSCs. Therefore, a film formation process with a non-equilibrium plasma brings great advances in producing a DSSC, and leads to considerable progress in solving global environmental problems. The high photovoltaic performance of DSSCs prepared using plasma techniques has been reported in many research groups. However, most of them utilized the techniques for cleaning and activating the surface of the porous TiO_2 layer prepared by conventional heating processes [39-44], and surface modification of the polymer counter-electrode. [45, 46] One of the most important requirements to enable the use of plastic substrates for DSSCs is to establish a low-temperature technique to form the porous TiO_2 layer. [47] In this study, we applied a novel plasma technique to form a porous TiO_2 layer on an FTO-coated substrate for a DSSC. However, we employed a glass substrate here, because the handmaid electrode caused to a non-homogeneous plasma distribution with micrometers of fine sparks because of a low resolution of the screen-printed grid pattern and damaged the plastic substrate during film formation. We further investigated the active plasma species to promote a necking process between TiO_2 particles during plasma irradiation by adjusting the volume fraction of the flowing mixture of nitrogen and oxygen gases.

2. Experimental

The procedure for preparing the electrode for a discharge is shown in Fig. 1(c). The grid patterns were screen-printed with a resistive paste (R-2010, Shoei Kagaku) on both faces of an aluminum plate, 50×25×0.6 mm^3 in size, and sintered at 1150 ˚C in air. Then, the contact points for the terminals were screen-printed with a conductive paste (D-4344, Shoei Kagaku) at the two ends of the grid, and sintered at 900 ˚C in air. The insulating paste (QM44, DuPont) was screen-printed to cover the whole grid layer, and sintered at 1000 ˚C in air. Finally, two lead wires were screw-clamped to complete the electrode. A sinusoidal wave from a function generator (WF1965, NF Co.) was applied to the electrode through a high-voltage power amplifier (Model 20/20C, Trek Inc.) up to 15 kV and 20 kHz. Fig. 1(d) shows a photograph of the electrode during discharge. A blue planar plasma originating from nitrogen gas in the air was induced along the grid pattern on the electrode. The energy of the plasma was estimated using a capacitor of 330 nF incorporated into the electric circuit of the discharge system. When the plasma was induced on the electrode, a typical rhombic Lissajous figure was displayed on the connected digital oscilloscope (TDS2024B, Tektronix Inc.). Assuming that the energy of a plasma in discharge is almost the same as that stored in the capacitor,

the energy was calculated from the area of the *Q*-*V* diagram in the figure. [48)]

A 0.1 M di-*n*-butyltin(IV) diacetate (DBTDA, Tokyo Kasei Kogyo) ethanol solution with an additive of ammonium fluoride (NH_4F, FUJIFILM Wako Pure Chemical) in the molar ratio of [NH_4F]/[DBTDA] = 1.6 was prepared for a source solution. The solution was sprayed by a nozzle (Lumina STA-6R-1mmϕ, Fuso Seiki) with a compressed air onto a heated glass substrate (Corning 1737). The mist was pyrolyzed on the substrate at a substrate temperature of 500 ˚C in air to form an FTO film with sheet resistance and average transmittance in the visible region of 10 Ω/sq and 80%, respectively. [29-38)] A 0.1 M of bis (2,4-pentanedionato) titanium(IV) oxide (Tokyo Kasei Kogyo) ethanol solution was sprayed onto an FTO glass substrate at 500 ˚C in air to deposit a dense TiO_2-buffer layer. [32, 33, 38)] A 0.1 M of TiO_2 suspension of the mixture of STS-02 (Ishihara Sangyo) and P25 (Degussa) with the molar ratio of [STS-02]/[P25] = 1.0 was sprayed onto the buffer layer at 150 ˚C in air to stack a porous TiO_2 layer with the thickness of 5 μm. Titanium (IV) tetraisopropoxide (Kanto Chemical) was diluted with 1.0 M of hydrogen peroxide (FUJIFILM Wako Pure Chemical) to prepare a 0.1 M titanium-peroxo complex (TTIP) precursor. [47, 49, 50)] The porous TiO_2 layer on the FTO-coated glass substrate was immersed in the TTIP precursor for 10 min, and dried in air. Then, the layer was set on the holder to face the electrode for a discharge. The distance between the porous TiO_2 layer and the electrode was fixed at 0.05 mm using a goniometer. After placing the holder within the enclosure connected to a flow meter, a non-equilibrium 2D plasma was induced under the flowing mixture of nitrogen and an oxygen gases with the volume fraction from N_2/O_2 = 100/0 to 0/100 and irradiated to the surface of the porous TiO_2 layer for 15 min. During the plasma irradiation, the gas mixture was supplied to the system at flow rate of 5 L/min. Since the plasma density decays exponentially under atmospheric pressure the procedure was repeated twice to form a 10 μm-thick porous TiO_2 layer for effective plasma treatment in the bulk. N719 (Ruthenium 535-bisTBA, FUJIFILM Wako Pure Chemical) dye was adsorbed on the surface of the porous TiO_2 layer by soaking the electrode in a 1×10^{-4} M ethanol solution at room temperature for 12 h. The amount of dye adsorbed on the porous TiO_2 layer was estimated by spectrophotometry. Finally, the dye-adsorbed TiO_2 electrode and platinum-coated glass electrode were clamped by clips, and then a drop of a mixture of anhydrous I^-/I_3^- electrolyte (0.6 M of 1,2-dimethyl-3-propylimidazolium iodide (Kanto Chemical), 0.1 M of lithium iodide (FUJIFILM Wako Pure Chemical), 0.5 M of 4-*tert*-butylpyridine (Tokyo Kasei Kogyo), 0.05 M of iodine (Kanto Chemical), and 0.2 M of guanidine thiocyanate (FUJIFILM Wako Pure Chemical) in acetonitrile (FUJIFILM Wako Pure Chemical)) was injected between the electrodes through a small gap using capillary force to fabricate a DSSC with an apparent area of 0.21 cm^2.

The current-voltage (*J*-*V*) characteristics of the DSSC were measured under 1 sun of quasi-sunlight of AM-1.5 and 100 mW/cm^2 (HAL-320, Asahi Spectra) directly irradiated to the cell. Electrochemical impedance was measured using the Electrochemical Test System (1470E and 1255B, Solartron) in the AC frequency range of 1×10^{-3} to 1×10^{6} Hz.

3. Results and discussion

Fig. 2 shows the surface morphology of the porous TiO_2 layers formed by irradiating the plasma induced under a flowing mixture of nitrogen and oxygen gases at various volume fractions. As shown in Fig. 2(a), the pores of the TiO_2 layer were fully covered with the TTIP precursor before irradiating with the plasma. A relatively flat surface originating from the shallow pores was observed for the layer formed under pure oxygen flow, or N_2/O_2=0/100. On the other hand, as the nitrogen gas concentration increased, a clear porous structure with a TiO_2 particle size of 10–20 nm was observed. We found that the oxidization of the TTIP precursor and the subsequent necking process between TiO_2 particles were effectively promoted by irradiating it with the plasma induced under a high nitrogen concentration.

X-ray diffraction (XRD) measurements were conducted to determine the oxidization process of the TTIP precursor during plasma irradiation. Fig. 3 shows the XRD patterns of the film formed by irradiating plasma onto the TTIP layer pre-coated on a glass substrate under a mixture of nitrogen and oxygen at various volume fractions. The (101) peak of the anatase TiO_2 phase was observed for the films formed under high nitrogen gas concentrations from N_2/O_2 = 70/30 to 99.8/0.2. We found that the crystallinity was the highest for the film formed under the gas flow of N_2/O_2 = 99.8/0.2, and that irradiating with the plasma species induced under higher nitrogen gas concentration was the key in forming a highly crystallized TiO_2 film. Considering the XRD patterns, a relatively flat surface on the porous TiO_2 layer formed under pure oxygen flow was attributed to the unreacted and/or intermediate products of the TTIP precursor left within the pores after the plasma treatment. In contract, a higher nitrogen concentration promoted the oxidization of the TTIP precursor and accelerated the necking process between TiO_2 particles. The porous surface morphology in Fig. 2(e) is supposed to originate from the fine necks of the highly crystallized anatase TiO_2 phase. After the plasma treatment, the amount of N719 dye adsorbed on the porous TiO_2 layer increased with increasing nitrogen concentration as shown in Table 1. This is attributed to the fact that the surface area of the porous TiO_2 layer increased owing to the decomposition of the TTIP precursor and subsequent volume shrinkage to produce the porous structure. On the other hand, under pure oxygen flow, the amount of the dye was less than others in gas fractions, revealing a lower decomposition rate of the TTIP precursor. However, the amount of dye adsorbed on the porous TiO_2 layer was estimated to be comparable to that formed by a conventional electric furnace. The amount of dye in this study was the typical value for a porous TiO_2 layer in a DSSC, corresponding to the roughness factor, i.e. the active surface area with respect to the apparent one, of approximately 1000. The results indicate that the porous TiO_2 layer formed by the novel plasma technique is acceptable for use in the working-electrode for DSSCs.

Table 1 shows the photovoltaic parameters of the DSSCs fabricated with the porous TiO_2 layer

formed with a non-equilibrium 2D plasma induced under a flowing mixture of nitrogen and oxygen with various volume fractions. Three cell parameters, the short circuit current density (J_{SC}), open circuit voltage (V_{OC}), and fill factor (FF) were enhanced with increasing nitrogen concentration. This is because some active plasma species were induced on the electrode to promote oxidation of the TTIP precursor. Furthermore, the necking process between TiO_2 particles was supposed to be accelerated by higher nitrogen concentrations to achieve smooth electrical transport within the porous TiO_2 layer. The energy of the plasma was calculated to be 4.8−5.0 J/s, and was comparable to that under all atmospheric conditions, which is high enough to decompose the precursor within a few seconds. The energy calculated here corresponds to that of the electrons in discharge. However, since the high-energy electrons collide with an atmospheric gas and generate a plasma, the energy is supposed to be comparable to that of plasma species induced on the electrode. Additionally, the temperature of the electrode in discharge was kept below 80 ˚C with a cooling water unit during film formation, and the UV-O_3 effect during the plasma irradiation can be ignored because it is restricted only to cleaning on the surface of the film. [39] We suppose that the decomposition of the TTIP precursor was not conducted thermally but by a chemical reaction between the precursor and active plasma species. Generally, the plasma species originating from pure nitrogen gas are reported as N_2, N, N_2^+ and N^+, which seem to be the key elements in decomposing the TTIP precursor. [51-54] However, the photovoltaic performance in this study did not show the maximum value for the cell prepared under pure nitrogen flow, or N_2/O_2 = 100/0. The conversion efficiency reached as high as 3.7 % for the cell prepared under the gas flow of N_2/O_2 = 99.8/0.2, indicating that the plasma species originating from the gas mixture are essential and that the N−O active plasma species strongly contributed to the oxidation of the TTIP precursor. Under atmospheric pressure, the gas mixture of nitrogen and oxygen induces mainly ten active plasma species: O, O^+, O_2, O_2^+, N, N^+, N_2, N_2^+, NO, and NO^+. [52, 53] As mentioned previously, anatase TiO_2 phase was detected in the XRD patterns and the photovoltaic performance was enhanced with an effective necking between TiO_2 particles under a higher nitrogen gas concentration. We suppose that NO and/or NO^+ plasma species contributed to the oxidation process to the TTIP precursor. Suetomi et al. reported that the amount of the excited N_2 metastable plasma initially increased with an increase in the nitrogen gas concentration under atmospheric pressure. [52, 53] Then, the excited N_2 metastable species collide with oxygen gas to generate the excited NO metastable plasma. They also reported that the concentration of the excited NO metastable plasma increased with increasing nitrogen gas concentration and reached a maximum at the volume fraction of N_2/O_2 = 99.8/0.2. We suppose that the excited NO metastable plasma played an important role in oxidizing the TTIP precursor to accelerate the necking process between the TiO_2 particles, resulting in effective electron transport within the cell. Considering the molecular structure of the titanium-peroxo complex, or the TTIP precursor, since the oxygen atoms are directly bonded to a titanium ion and form TiO_6 octahedra polycondensation, the molecular structure is advantageous for

crystallization under a low oxygen gas concentration. [49] Furthermore, due to a high-energy plasma, local heating only on the surface of the film is supposed to be an additional mechanism for crystallization, although the detailed mechanism has not been clarified yet. However, as shown in Table 1, the photovoltaic performance of the cell with the porous TiO_2 layer formed by the plasma technique was lower than that of the general DSSC prepared by a conventional electric furnace at 500 ˚C. The photovoltaic parameters of the cell prepared under the gas mixture flow of N_2/O_2 = 99.8/0.2 are comparable to those prepared by the electric furnace at 300 ˚C in air.

Electrochemical impedance measurements were conducted to investigate the effect of the oxidation of the TTIP precursor and the subsequent crystallization on the internal resistance in the cell. Fig. 4 shows the Nyquist plot of the impedance measurement of DSSCs. The spectrum displayed in the figure was estimated using the Z-View plot software installed in the measurement system according to the equivalent electric circuit. [55] Each spectrum consisted of a series resistance, R_0, and four arcs, ω_1–ω_4. R_0 and the real parts of the four arcs are summarized in Table 2. R_0 is a series resistance, corresponding to the sum of that of the FTO transparent conductive layer and the TiO_2 buffer layer, which is comparable in all cells because the double layer was formed by the SPD technique before plasma treatment. Then, we treated the value of R_0 as the series resistance of the TCO layer. [38] R_1 is the interface resistance at the porous TiO_2/TCO and/or the Pt counter-electrode/electrolyte. However, because the interface at the Pt counter-electrode/electrolyte is under the same conditions in all cells, the value of R_1 reflects the interface resistance at the porous TiO_2/TCO. Except for the cell prepared under pure oxygen gas flow, the value of R_1 did not depend on the gas fractions during film formation, and was estimated to be 13−16 Ω, which is comparable to that of the cell prepared in a conventional electric furnace. This is because the homojunction between the porous- and buffer-TiO_2 layer was easily produced during plasma treatment. R_2 is the TiO_2 interparticle resistance within the porous layer and was estimated to be 80 Ω for the cell prepared under the mixture gas flow of N_2/O_2 = 70/30. The value was effectively reduced with increasing nitrogen gas concentration, and reached as low as 32 Ω when prepared under the gas ratio of N_2/O_2 = 99.8/0.2. As mentioned above, the NO metastable active plasma induced under the higher nitrogen gas concentrations accelerated the necking process between TiO_2 particles and produced an effective electron path between the TiO_2 particles. This is supported by the XRD measurements for the films formed under higher nitrogen gas concentrations. Almost the same behavior of the atmospheric dependence was detected in R_3, the interface resistance at the porous TiO_2 layer/dye/electrolyte. The value of R_3 was strongly correlated to R_2. Since the amount of dye adsorbed on the porous TiO_2 layer was comparable in all cells, we suppose that the lower interface resistance was attributed to the smooth electron transport between TiO_2 particles, leading to effective photoelectron injection from the dye molecule to the porous TiO_2, which reduced the recombination process within the cell. R_4 corresponds to the resistance of ionic diffusion in the electrolyte. The value of R_4 decreased with

increasing nitrogen gas concentration, which seems to be due to the lower recombination rate of photoelectrons for the cell prepared under the higher nitrogen gas concentration as mentioned in R_3. Regarding the values of R_1, R_2, R_3, and R_4 for the cell prepared under the gas ratio of N_2/O_2 = 99.8/0.2, the interface resistance remains close to that for the cell prepared in an electric furnace at 300 ˚C in air. Generally, the photovoltaic performance is directly influenced by the internal resistance. The internal resistance in the cell fabricated in this study was higher than that in the cell prepared in an electric furnace at 500 ˚C in air, indicating that the oxidization of the TTIP precursor and the subsequent necking process between TiO_2 particles was not completed using this plasma technique. We suppose this is because the active plasma species did not fully reach to bulk of the porous TiO_2 layer during film formation due to a thin and a planar non-equilibrium plasma with a short lifetime under atmospheric pressure. Further improvement in effective plasma treatment on the substrate is required in the novel plasma technique to fabricate a high-performance DSSC.

4. Conclusion

A porous TiO_2 layer was formed by a novel film formation technique with a non-equilibrium 2D plasma. Under the flowing mixture of gases of nitrogen and oxygen at the volume fraction of N_2/O_2 = 99.8/0.2, an active NO metastable plasma was induced to promote the oxidization of the titanium-peroxo complex precursor, which accelerated the necking process between TiO_2 particles in forming a porous TiO_2 layer. The layer was employed as the working-electrode for a DSSC. The internal resistance in this cell was higher than that in the cell prepared by an electric furnace at 500 ˚C in air, indicating that the necking process between TiO_2 particles was not completed. We suppose this is because most of the active plasma species could not reach the bulk of the porous TiO_2 layer during plasma irradiation. However, due to the merits of a non-equilibrium 2D plasma, after improving the system for effective plasma treatment to the substrate, the novel film formation technique brings great advances in producing DSSCs, and leads to considerable progress in solving global environmental problems.

Acknowledgment

This work was supported by JSPS KAKENHI Grant Number JP20K03916.

References

1) T. Homola, J. Matoušek, V. Medvecká, A. Zahoranová, M. Kormunda, D. Kováčik, and M. Černák, Appl. Surf. Sci. **258**, 7135 (2012).

2) L. Bonova, A. Zahoranova, D. Kovacik, M. Zahoran, M. Micusik, and M. Cernak, Mirko, Appl. Surf. Sci. **331**, 79 (2015).

3) Y. F. Hong, J. G. Kang, H. Y. Lee, H. S. Uhm, H. S.; Moon, and Y. H. Park, Lett. Appl. Microbio. **48**, 33 (2009).

4) S. Lerouge, M. R. Wertheimer, R. Marchand, M. Tabrizian, and K. H. Yahia, J. Biomedical Mater. Res. **51**, 128 (2000).

5) K. D. Weltmann, E. Kindel, T. von Woedtke, M. Haehnel, M. Stieber, and R. Brandenburg, Pure Appl. Chem. **82**, 1223 (2010).

6) K. Takahashi, H. Akahoshi, C. Charles, R.W. Boswell, A. Ando, Phys. Plasmas **24**, 084503 (2017).

7) K. Takashima, and T. Kaneko, Plasma Sources Sci. Tech. **26**, 065018 (2017).

8) H. Yamasaki, Y. Koizumi, T. Kuroki, and M. Okubo, Energies **12**, 2717 (2019).

9) Y. Osaka, K. Iwai, T. Tsujiguchi, A. Kodama, X. Li, and H. Huang, Separa. Purifi. Tech. **215**, 108 (2019).

10) K. N. Kim, S. M. Lee, A. Mishra, and G. Y. Yeom, Thin Solid Films **598**, 315 (2016).

11) E. Mudra, M. Streckova, D. Pavlinak, V. Medvecka, D. Kovacik, A. Kovalcikova, P. Zubko, V. Girman, Z. Dankova, and V. Koval, and J. Duzsa, Appl. Surf. Sci. **415**, 90 (2017).

12) Y. Okazaki, Yasumasa, Y. Wang, H. Tanaka, M. Mizuno, K. Nakamura, H. Kajiyama, H. Kano, K. Uchida, F. Kikkawa, M. Hori, and S. Toyokuni, J. Clinic. Biochem. Nutri. **55**, 207 (2014).

13) A. Zahoranova, L. Hoppanova, J. Simoncicova, Z. Tucekova, V. Medvecka, D. Hudecova, B. Kalinakova, D. Kovacik, and M. Cernak, Plasma Chem. Plasma Process. **38**, 969 (2018).

14) W.Tian, K. Tachibana, and M. Kushner, J. Phys. D **47**, 055202 (2014).

15) A. Tamura, A. Matsumoto, K. Fukami, N. Nishi, and T. Sakka, J. Appl. Phys. **117**, 173304 (2015).

16) T. Sato, S. Uehara, R. Kumagai, T. Miyahara, M. Oizumi, T. Nakatani, S. Ochiai, T. Miyazaki, H. Fujita, S. Kanazawa, K. Ohtani, A. Komiya, T. Kaneko, T. Nakajima, M. Tinguely, and M. Farhat, Inter. J. Plasma Environ. Sci. Tech. **12**, 44 (2019).

17) S. V. Vladimirov, S. A. Khrapak, M. Chaudhuri, and G. E. Morfill, Phys. Rev. Lett. **100**, 055002 (2008).

18) S. Nakahara, S. Stauss, T. Kato, T. Sasaki, and K. Terashima, J. Appl. Phys. **109**, 123304 (2011).

19) S. Himeno, T. Kato, K. Urabe, S. Stauss, S. Kato, H. Muneoka, M. Baba, T. Suemoto, and K. Terashima, IEEE Trans. Plasma Sci. **42**, 2630 (2014).

20) C. Ishii, S. Stauss, K. Kuribara, K. Urabe, T. Sasaki, and K. Terashima, Diamond Rel. Mater. **59**, 40 (2015).

21) A. Garcia, X. Buelna, E. Popov, and J. Eloranta, J. Chem. Phys. **145**, 124504 (2016).

22) J. Hopwood, O. Minayeva, and Y. Yin, J. Vac. Sci. Tech. B **18**, 2446 (2000).
23) R. Degl'Innocenti, S. Reidt, A. Guarino, D. Rezzonico, G. Poberaj, and P. Gunter, J. Appl. Phys. **100**, 113121 (2006).
24) B. Hopp, T. Smausz, T. Csizmadia, C. Vass, T. Csako, and G. Szabo, J. Laser Micro/Nanoeng. **5**, 80 (2010).
25) S. Tao, Y. Zhou, B. Wu, and Y. Gao, Appl. Surf. Sci. **258**, 7766 (2012).
26) V. Y. Shanygin, R. K. Yafarov, Semiconductors **47**, 469 (2013).
27) Y. Sonohara, Y. Shibayama, K. Kusama and M. Okuya, Proc. The 24 Japan-Korea International Seminar on Ceramics, 2007, p.445.
28) M. Okuya, K. Nabeta, Y. Shibayama, S. Kanezashi, M. Tan, M. Iyoda, M. Shikatani, Y. Sonohara and I. Yagi, Appl. Phys. Exp. **7**, 015501 (2014).
29) M. Okuya, S. Kaneko, K. Hiroshima, I. Yagi, and K. Murakami, J. Euro. Ceram. Soc. **21**, 2099 (2001).
30) M. Okuya, K. Nakade, and S. Kaneko, Sol. Energy Mater. Sol. Cells **70**, 415 (2002).
31) M. Okuya, D. Osa, and S. Kaneko, Key Eng. Mater. **228-229**, 247 (2002).
32) M. Okuya, K. Nakade, D. Osa, T. Nakano, and S. Kaneko, J. Photochem. Photobio. A Chem. **164**, 167 (2004).
33) M. Okuya, N. Horikawa, T. Kosugi, G.R.A. Kumara, J. Madarász, S. Kaneko, G. Pokol, Solid State Ionics **172**, 527 (2004).
34) M. Okuya, K. Ohashi, T. Yamamoto, and J. Madarász, Electrochemistry **76**, 132 (2008).
35) T. Yamamoto, K. Ohashi, and M. Okuya, Trans. Mat. Res. Jpn. **35**, 409 (2010).
36) G. R. A. Kumara, C. S. K. Ranasinghe, E. N. Jayaweera, H. M. N. Bandara, M. Okuya and R. M. G. Rajapakse, J. Phys. Chem. C **118**, 16479 (2014).
37) R. Otsuka, T. Endo, T. Takano, S. Takemura, R. Murakami, R. Muramoto, J. Madarász and M. Okuya, Jpn. J. Appl. Phys. **54**, 08KF03 (2015).
38) M. Okuya, J. Sato, T. Endo, R. Iwaki, S. Takemura, R. Muramoto, V. Nagygyörgy, J. Madarász, S. Nakao, N. Yamada, E. Sakai, T. Hitosugi, and T. Hasegawa, J. Am. Ceram. Soc. **101**, 5071 (2018).
39) T. Yamaguchi, N. Tobe, D. Matsumoto, T. Nagai, and H. Arakawa, Sol. Ener. Mat. Sol. Cells **94**, 812 (2010).
40) X. Xin, M. Scheiner, M. Ye, and Z. Lin, Langmuir **27**, 14594 (2011).
41) M. Ye, X. Xin, C. Lin, and Z. Lin, Nano Lett. **11**, 3214 (2011).
42) W. Wu, T. Shih, P. Chen, J. Ting, J. Chen, J. Electrochem. Soc., **158**, K101 (2011).
43) H. Kim, J. Kim, and B. Hong, Appl. Surf. Sci. **274**, 171 (2013).
44) V. Dao, L. Larina, and H. Choi, J. Electrochem. Soc. **161**, H896 (2014).
45) S. Das, P. Sudhagar, V. Verma, D. Song, E. Ito, S. Lee, Y. Kang, and W. Choi, Adv. Functional Mater. **21**, 3729 (2011).

46) D. Dao, C. Tran, S. Ko, and H. Choi, J. Mater. Chem. A **1**, 4436 (2013).

47) M. Hočevar, U. Opara Krašovec, and M. Topič, J. Sol-Gel Sci. Tech. **68**, 67 (2013).

48) H. E. Wagner, R. Brandenburg, K. V. Kozlov, A. Sonnenfeld, P. Michel, and J. F. Behnke, Vacuum **71**, 417 (2003).

49) S. I. Seok, B. Y. Ahn, N. C. Pramanik, and H. Kim, J. Am Ceram. Soc. **89**, 1147 (2006).

50) M. Drev, U. O. Krašovec, M. Hočevar, M. Berginc, M. K. Maček, and M. Topič, J. Sol-Gel Sci. Tech. **59**, 245 (2011).

51) Y. Ishii, T. Shibata, Y. Yoshino, H. Ichimura, K. Kobayashi, J. Ceram. Soc. Jpn. **100**, 1184 (1992).

52) K. H. Becker, U. Kogelschatz, K. H. Schoenbach, and R. J. Barker, *Non-Equilibrium Air Plasmas at Atmospheric Pressure* (Institute of Physics Publishing, 2005) p.168.

53) E. Suetomi, T. Muzukoshi, K. Fukazawa, A. Saito, Konica Minolta Technology Report **3**, 80 (2006) [in Japanese].

54) E. Suetomi, T. Mizukoshi, K. Fukazawa, A. Saito, IEEJ Trans. Fund. Mater. **127**, 423 (2007).

55) T. Hoshikawa, M. Yamada, R. Kikuchi, and K. Eguchi, J. Electrochem. Soc. **152**, E68 (2005).

Figure Captions

Fig. 1 Electrode for dielectric barrier discharge to induce non-equilibrium 2D plasma: schematic representation of (a) conventional coplanar type electrode and (b) novel vertical type electrode, (c) procedure to prepare vertical type electrode, and (d) photograph of handmaid electrode before (top) and after (bottom) applying AC bias of 15 kV and 20 kHz in air.

Fig. 2 Surface morphology of porous TiO_2 layers formed by irradiating with plasma induced under a flowing mixture of nitrogen and oxygen gases with various volume fractions: (a)as-deposited, (b)N_2/O_2=0/100, (c)N_2/O_2=70/30, (d)N_2/O_2=99/1, (e)N_2/O_2=99.8/0.2, and (f)N_2/O_2=100/0.

Fig. 3 XRD patterns of film formed by irradiating plasma onto TTIP precursor pre-coated on a glass substrate under mixture of nitrogen and oxygen gases at various volume fractions.

Fig. 4 Nyquist plot of impedance spectra of DSSCs with porous TiO_2 layers formed by irradiating with plasma induced under a flowing mixture of nitrogen and oxygen gases at various volume fractions. Film formation by electric furnace in air was conducted as a reference. The inset shows fitting arcs to the spectrum of cell prepared under gas mixture flow of N_2/O_2 = 99.8/0.2 using Z-view plot software according to equivalent circuit in DSSC. [55)]

Table 1 Amount of N719 dye and photovoltaic parameters of DSSC fabricated with porous TiO_2 layer formed by irradiating with plasma induced under a flowing mixture of nitrogen and oxygen gases at various volume fractions. Film formation by electric furnace in air was conducted as a reference.

Table 2 Series resistance and real part of four arcs in impedance spectra of DSSCs fabricated with porous TiO_2 layer formed by irradiating with plasma induced under a flowing mixture of nitrogen and oxygen gases at various volume fractions. Film formation by electric furnace in air was conducted as a reference. Fitting to each spectrum was conducted using Z-view plot software according to equivalent circuit in DSSC. [55)]

(a)

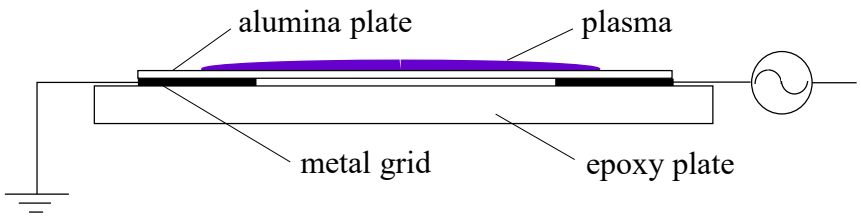
alumina plate
plasma
metal grid
epoxy plate

(b)

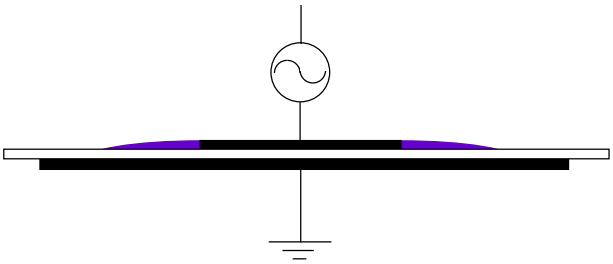

(c)

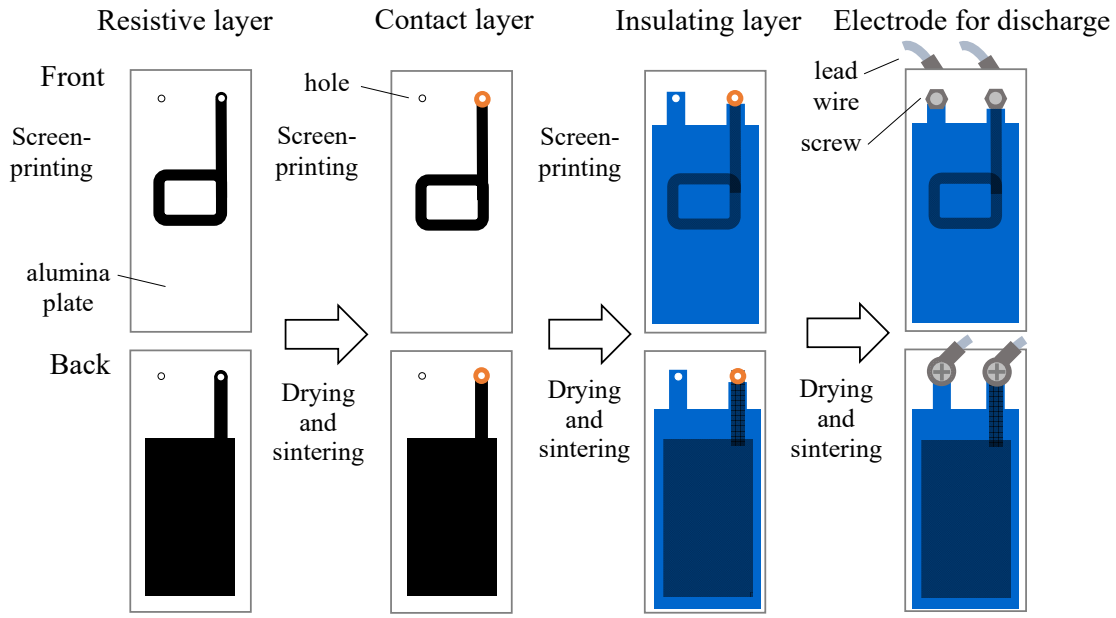
Resistive layer
Contact layer
Insulating layer
Electrode for discharge
Front
Screen-printing
alumina plate
Back
Drying and sintering
hole
Screen-printing
Drying and sintering
Screen-printing
Drying and sintering
lead wire
screw

(d)

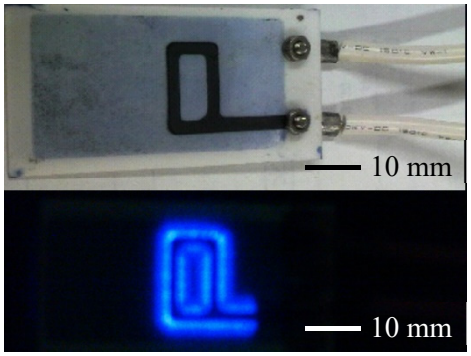

Fig. 1 Electrode for dielectric barrier discharge to induce non-equilibrium 2D plasma: schematic representation of (a) conventional coplanar type electrode and (b) novel vertical type electrode, (c) procedure to prepare vertical type electrode, and (d) photograph of handmaid electrode before (top) and after (bottom) applying AC bias of 15 kV and 20 kHz in air.

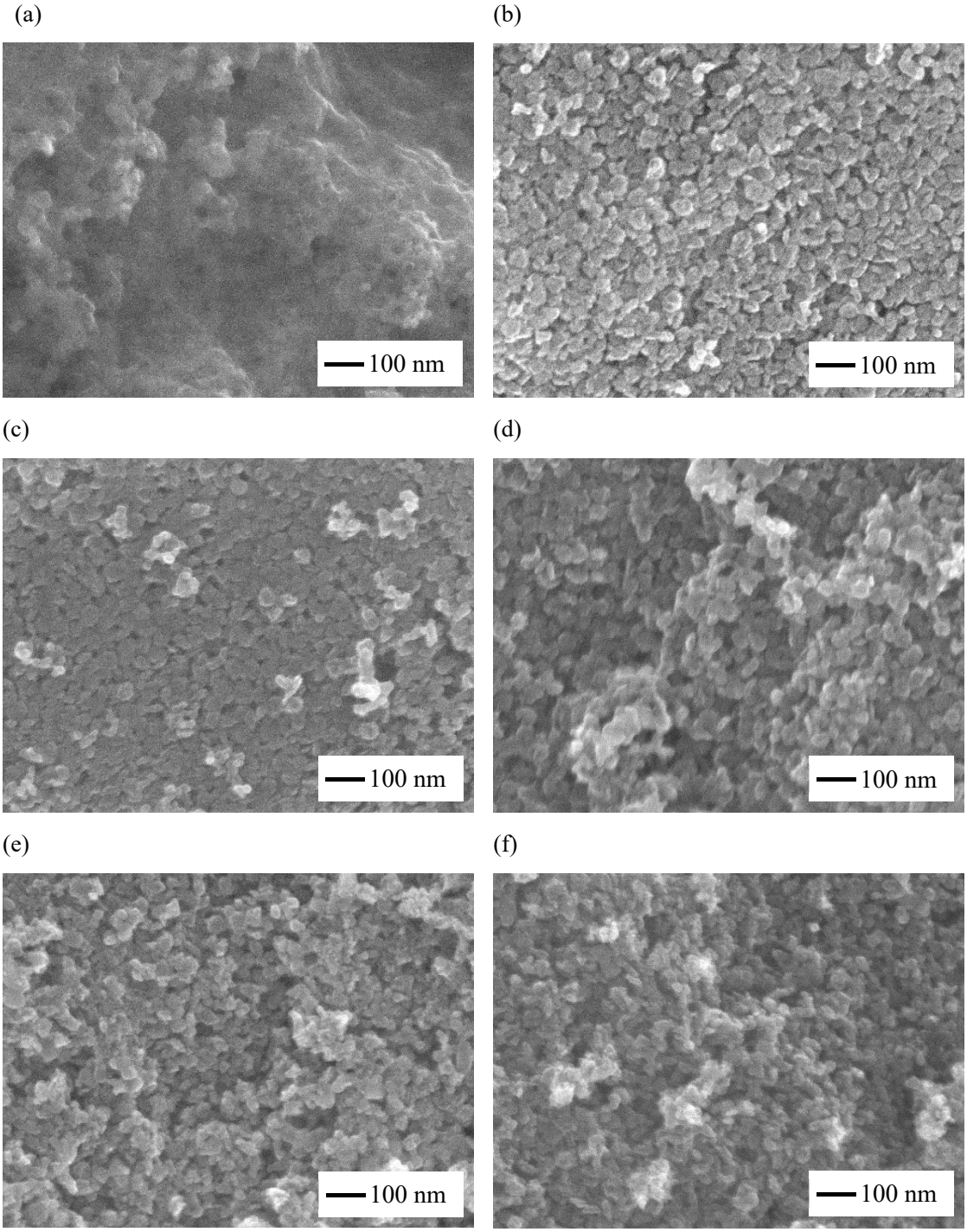

Fig. 2 Surface morphology of porous TiO_2 layers formed by irradiating with plasma induced under a flowing mixture of nitrogen and oxygen gases with various volume fractions: (a)as-deposited, (b)N_2/O_2=0/100, (c)N_2/O_2=70/30, (d)N_2/O_2=99/1, (e)N_2/O_2=99.8/0.2, and (f)N_2/O_2=100/0.

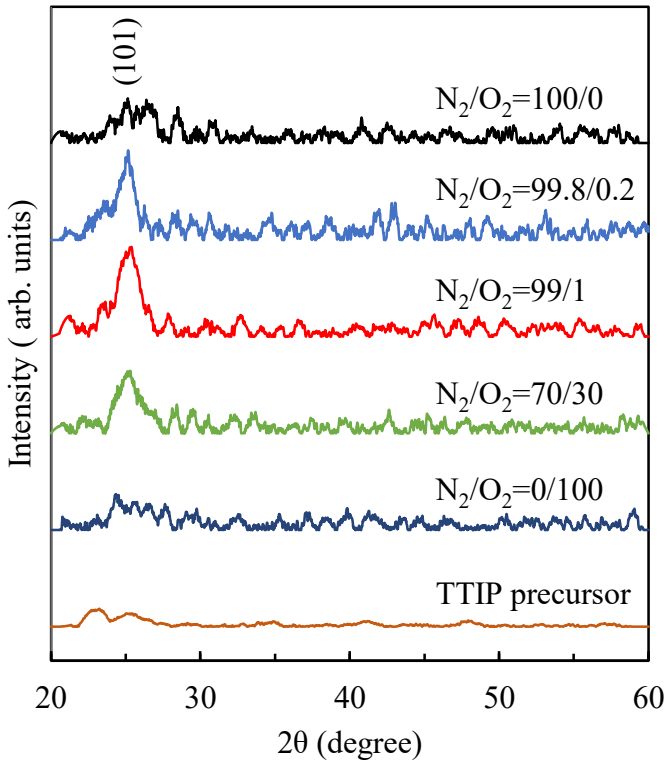

Fig. 3 XRD patterns of film formed by irradiating plasma onto TTIP precursor pre-coated on a glass substrate under mixture of nitrogen and oxygen gases at various volume fractions.

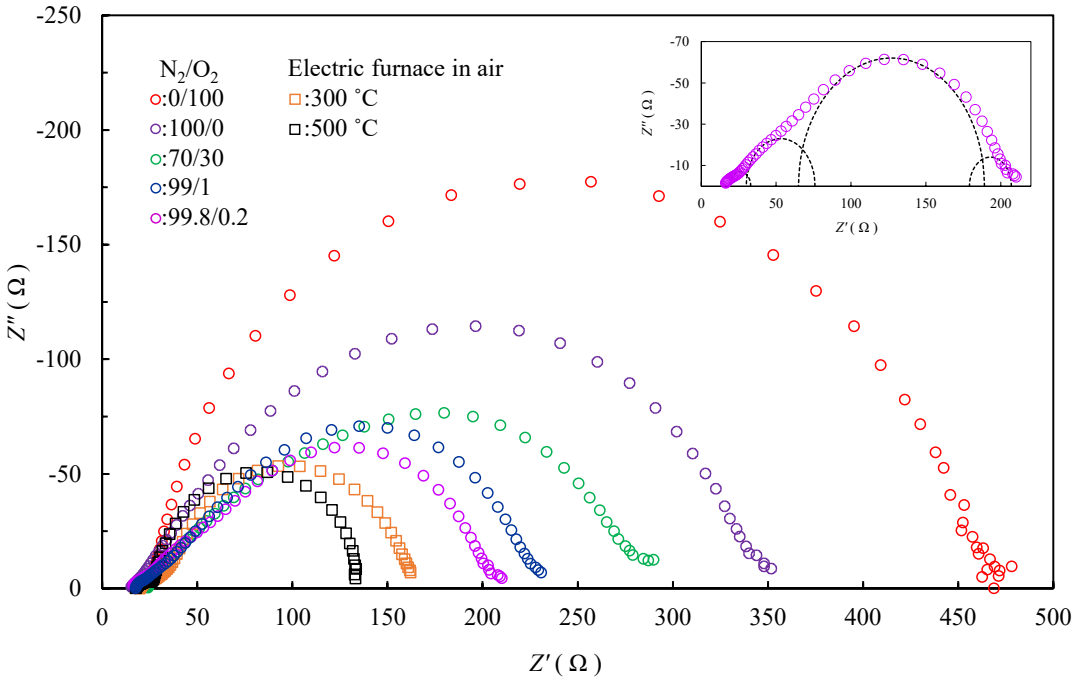

Fig. 4 Nyquist plot of impedance spectra of DSSCs with porous TiO_2 layers formed by irradiating with plasma induced under a flowing mixture of nitrogen and oxygen gases at various volume fractions. Film formation by electric furnace in air was conducted as a reference. The inset shows fitting arcs to the spectrum of cell prepared under gas mixture flow of $N_2/O_2 = 99.8/0.2$ using Z-view plot software according to equivalent circuit in DSSC. [55)]

Table 1　Amount of N719 dye and photovoltaic parameters of DSSC fabricated with porous TiO_2 layer formed by irradiating with plasma induced under a flowing mixture of nitrogen and oxygen gases at various volume fractions.　Film formation by electric furnace in air was conducted as a reference.

		Volume fraction N_2/O_2	N719 dye ($\times 10^{-7}$ mol/cm^2)	J_{SC} (mA/cm^2)	V_{OC} (V)	FF	η (%)
plasma		0/100	1.32	1.4	0.61	0.38	0.3
		70/30	1.82	4.8	0.72	0.67	2.3
		99/1	1.93	5.4	0.78	0.67	2.8
		99.8/0.2	1.93	6.4	0.79	0.73	3.7
		100/0	1.72	3.8	0.73	0.71	2.0
Electric furnace (˚C)	300	air	1.72	8.0	0.74	0.68	4.1
	500	air	1.93	15.8	0.71	0.68	7.6

Table 2　Series resistance and real part of four arcs in impedance spectra of DSSCs fabricated with porous TiO_2 layer formed by irradiating with plasma induced under a flowing mixture of nitrogen and oxygen gases at various volume fractions.　Film formation by electric furnace in air was conducted as a reference.　Fitting to each spectrum was conducted using Z-view plot software according to equivalent circuit in DSSC. [55)]

		Volume fraction N_2/O_2	R_0 (Ω)	R_1 (Ω)	R_2 (Ω)	R_3 (Ω)	R_4 (Ω)
plasma		0/100	21	20	108	360	54
		70/30	23	16	80	156	34
		99/1	21	14	50	134	32
		99.8/0.2	20	13	32	131	28
		100/0	15	14	84	232	52
Electric furnace (˚C)	300	air	19	10	24	110	18
	500	air	17	7	12	102	6